

---

Article type : Original

## The IKK $\beta$ -USP30-ACLY Axis Controls Lipogenesis and Tumorigenesis

Li Gu <sup>#,1,2</sup>, Yahui Zhu <sup>#,1,2</sup>, Xi Lin <sup>1,2</sup>, Bingjun Lu <sup>1,2</sup>, Xinyi Zhou <sup>1,2</sup>, Feng Zhou <sup>3,4</sup>, Qiu Zhao <sup>3,4</sup>, Youjun Li <sup>1,2,\*</sup>

<sup>1</sup> Hubei Key Laboratory of Cell Homeostasis, College of Life Sciences, Wuhan University, Wuhan 430072, China

<sup>2</sup> Medical Research Institute, School of Medicine, Wuhan University, Wuhan 430071, China

<sup>3</sup> Department of Gastroenterology, Zhongnan Hospital of Wuhan University School of Medicine, Wuhan 430071 China;

<sup>4</sup> Hubei Clinical Center and Key Laboratory for Intestinal and Colorectal Diseases, Wuhan 430071, China;

# These authors contributed equally to this work.

\*Correspondence: [liy7@whu.edu.cn](mailto:liy7@whu.edu.cn)

This article has been accepted for publication and undergone full peer review but has not been through the copyediting, typesetting, pagination and proofreading process, which may lead to differences between this version and the [Version of Record](#). Please cite this article as [doi: 10.1002/HEP.31249](https://doi.org/10.1002/HEP.31249)

This article is protected by copyright. All rights reserved

---

**Abbreviations:** ACC, acetyl-CoA carboxylase; ACLY, ATP citrate lyase; DEN, Diethylnitrosamine; FA, Fatty Acids; FASN, fatty acid synthase; HCC, hepatocellular carcinoma; HIF1, Hypoxia Inducible Factor 1; HSC, Hepatic Stellate Cell; IKK $\beta$ , I $\kappa$ B kinase  $\beta$ ; IL-6, Interleukin 6; JMJD3, lysine demethylase 6B; KLF4, kruppel-like factor 4; mTORC1, Mammalian Target of Rapamycin Complex 1; NAFLD, Nonalcoholic Fatty Liver Disease; NASH, Non-Alcoholic Steatohepatitis; NF- $\kappa$ B, Nuclear Factor kappa B; NSCLC, Non-Small-Cell Lung Carcinoma; PCAF, P300/Calcium-Binding Protein (CBP) Associated Factor; PD-L1, Programmed Death-Ligand 1; Pyruvate Kinase M2 (PKM2); RCC, Renal Cell Carcinoma; SCD, stearoyl-CoA desaturase; SIRT2, Sirtuin 2; SREBP1a, Sterol Regulatory Element Binding Transcription Factor 1; STAT3, Signal Transducer and Activator of Transcription 3; TAMs, Tumor-Associated Macrophages; TG, Triglyceride; TNF $\alpha$ , Tumor Necrosis Factor  $\alpha$ ; TSC1, Tuberous Sclerosis Complex 1; UBR4, Ubiquitin protein ligase E3 component n-recognin 4; USP30, Ubiquitin-Specific Peptidase 30.

**Financial Support:**

This work was supported by grants from the National Nature Science Foundation of China (81772609, 81902843), and China Postdoctoral Science Foundation (2019T120681, 2019M652702).

**Conflict of interest:**

The authors declare no competing interests.

---

## Abstract

Hepatocellular carcinoma (HCC) is a leading cause of cancer-related death that develops as a consequence of obesity, cirrhosis and chronic hepatitis. However, the pathways along which these changes occur remain incompletely understood. In this study, we show that the deubiquitinase USP30 is abundant in HCCs that arise in mice maintained on high fat diets (HFDs). IKK $\beta$  phosphorylated and stabilized USP30, which promoted USP30 to deubiquitinate ATP citrate lyase (ACLY) and fatty acid synthase (FASN). IKK $\beta$  also directly phosphorylated ACLY and facilitated the interaction between USP30 and ACLY and the latter's deubiquitination. In HCCs arising in DEN/CCl<sub>4</sub>-treated mice, USP30 deletion attenuated lipogenesis, inflammation and tumorigenesis irrespective of diet. The combination of ACLY inhibitor and PD-L1 antibody largely suppressed chemical-induced hepatocarcinogenesis. The IKK $\beta$ -USP30-ACLY axis was also found to be upregulated in human HCCs. *Conclusion:* This study identifies a new IKK $\beta$ -USP30-ACLY axis that plays an essential and wide-spread role in tumor metabolism and may be a potential therapeutic target in HCC.

---

## Introduction

HCC, the fifth most common cancer world-wide and the second cause of tumor-associated death, progresses through a series of steps, including the re-programming of cellular metabolism.<sup>(1,2)</sup> Accumulating evidence has demonstrated that lipid metabolism is substantially reprogrammed in tumorigenesis.<sup>(3)</sup> Lipid synthesis, uptake and storage are usually up-regulated in hepatocarcinogenesis, thus suggesting that targeting lipid metabolism might be a promising cancer therapy.<sup>(4, 5)</sup>

Nonalcoholic fatty liver disease (NAFLD), which is associated with the widespread production of inflammatory cytokines such as TNF- $\alpha$  and IL-6, plays an important role in HCC progression.<sup>(6)</sup> In addition to affecting tumor cells directly, these can also influence the tumor microenvironment which contains a variety of immunologically active cells, including Kupffer cells, T cells, antigen-presenting cells and hepatic stellate cells (HSCs).<sup>(7)</sup>

Ubiquitin-specific peptidase 30 (USP30), which mainly localizes to mitochondria, antagonizes mitophagy driven by Parkin and Pink1 and regulates mitochondrial morphology.<sup>(8)</sup> USP30 opposes Parkin-dependent ubiquitylation of TOM20 and restricts BAX/BAK-induced cell apoptosis.<sup>(9)</sup> Hence USP30 inhibition might be beneficial for the treatment of certain mitochondrial disorders.<sup>(8,10)</sup> USP30 is a deubiquitinase that preferentially removes Lys6- and Lys11-(K6/11) linked as well as Lys48 and Lys63-linked ubiquitination (Ub) chains.<sup>(11)</sup> The crystal structure of Lys6-linked diubiquitin of USP30 has been used to generate a model to explain the preference in K6-linkage deubiquitination of USP30.<sup>(12)</sup> However, no known role for USP30 in lipogenesis and/or tumorigenesis has been previously identified.

The I $\kappa$ B kinase  $\beta$  (IKK $\beta$ ) is a central element of the canonical NF- $\kappa$ B signaling pathway that mediates inflammation and oncogenesis.<sup>(13)</sup> Upon stimulation, I $\kappa$ B is phosphorylated by the IKK complex (IKK $\alpha$ , IKK $\beta$ , IKK $\gamma$ ) and degraded. This allows NF- $\kappa$ B to translocate into the nucleus where it activates its transcriptional program.<sup>(14)</sup> In addition to I $\kappa$ B, IKK $\beta$  directly phosphorylates numerous other substrates that either promote or repress tumorigenesis. The tumor suppressor TP53 restricts the activation of the IKK $\beta$ -NF- $\kappa$ B pathway by repressing glycolysis.<sup>(15)</sup> Prolonged IKK $\beta$  inhibition also depletes circulating T-regs and enhances antitumor responses.<sup>(16)</sup> In contrast,

---

IKK $\beta$  phosphorylates FOXO3a and TSC1, respectively, which leads to FOXO3a degradation, enhanced angiogenesis, mTORC1 activation and the promotion of breast cancer growth.<sup>(17, 18)</sup> Finally, in the DEN/CCL<sub>4</sub> model of HCC, IKK $\beta$  orchestrates an antagonistic proliferative cross-talk that is notable for a marked inhibition in hepatocarcinogenesis but an increased tumor burden that is largely the result of hepatocyte and hematopoietic-derived Kupffer cell expansion.<sup>(19)</sup>

ATP-citrate lyase (ACLY) is a cytosolic protein that catalyzes the formation of acetyl-CoA and oxaloacetate from citrate and coenzyme A in the presence of ATP.<sup>(20)</sup> It is thus a critical enzyme that links glucose catabolism, oxidative phosphorylation and lipogenesis and furnishes the initial substrate for fatty acid and cholesterol biosynthesis.<sup>(21)</sup> ACLY is highly expressed in many tumors, such as lung cancer, breast cancer, liver cancer and colon cancer.<sup>(22)</sup> ACLY knockout mice are embryonic lethal while heterozygous mice are healthy and demonstrate no difference in lipid synthesis compared to wild type (WT) mice.<sup>(23)</sup> ACLY is transcriptionally regulated by SREBP1a and can undergo many post-translational modifications,<sup>(24)</sup> including phosphorylation by AKT, nucleoside diphosphate kinase, cAMP-dependent protein kinase and Cyclin E;<sup>(25,26)</sup> acetylation by P300/Calcium-Binding Protein (CBP)-associated factor (PCAF) and deacetylation by Sirtuin 2 (SIRT2). Many of these modifications promote lipid synthesis and tumor growth.<sup>(27)</sup> In contrast, degradation of ACLY by Cullin 3-KLHL25 and UBR4 ubiquitination leads to tumor suppression.<sup>(27, 28)</sup> However, a functional role for ACLY deubiquitination has not been previously described.

In this study, we demonstrate that the mitochondrial deubiquitylase USP30 plays important roles in the lipogenesis and HFD-driven HCC. We identify that IKK $\beta$  phosphorylates USP30 and ACLY and that, as a result, USP30 promotes deubiquitination of ACLY. In mice, Usp30 knockout largely attenuates DEN-induced mouse hepatocarcinogenesis and inflammation in a manner that is uninfluenced by HFDs. Targeting ACLY using the inhibitor ETC1002 (Bempedoic Acid) and tumor immunology on PD-L1 abundantly represses liver tumorigenesis.

---

## Materials and Methods

### PLASMIDS AND CONSTRUCTS

The open reading frames of human IKK $\beta$ , USP30 and ACLY were amplified by PCR and cloned into pHAGE-CMV-MCS-PGK-3 $\times$ Flag and pCMV-HA vectors. Mutations in the ubiquitin, USP30 and ACLY cDNA sequences were generated by overlap extension PCR. Human IKK $\beta$ , ACLY and FASN shRNA vectors were obtained from GENECHM (Shanghai, China). Adeno-associated virus (AAV) vectors were obtained from Yan Wang (College of Life Science, Wuhan University). Primers used in this study are listed in Supplementary Table S1. Transfection and the establishment of stable cell lines were performed as previously described.<sup>(29)</sup>

Cycloheximide (R750107), Glutaraldehyde (G7651), proteasome inhibitor MG132 (M8699) and autophagy inhibitor 3-methyladenine (3-MA) (M9281) were purchased from Sigma-Aldrich. Mouse anti-PD-L1 antibody (BP0101) was purchased from Bio X Cell. ETC1002 (HY-12357) and phosphatase inhibitor cocktail (HY-K0021) were purchased from Med Chem Express (MCE). SC-514 (S4907), Anti-HA and anti-FLAG affinity agarose beads were purchased from Selleck (Houston, USA).

### METABOLIC ASSAYS

Serum TG levels were measured using the Infinity Triglycerides Reagent (Thermo Scientific). Fatty acids levels were determined with a Biovision ELISA kit (BioVision, Milpitas, CA, USA) according to the manufacturer's instruction.

Isotope experiments were performed as previously described.<sup>(30)</sup> Briefly, <sup>3</sup>H-acetic acid (1.59 Ci/mmol, Perkin Elmer, 37 KBq/ml) was added to the wells and incubated at 37°C overnight. Then cells were disrupted with lysis buffer (see above) and incubated at 37°C for 30 min. Organic extraction was performed in chloroform following the protocol of Bligh and Dyer and lipid-soluble products were measured by scintillation counting (Tri-Carb 2910 TR, Perkin Elmer).<sup>(31)</sup>

For ATP analysis, 5 $\times$ 10<sup>5</sup> cells were collected and extracted in 100 $\mu$ l of the ATP Assay Buffer

---

(Biovision). Particulate matter was pelleted at 12,000 rpm for 5 min and the supernatant was used for ATP assay. The reaction mixture was incubated for 30 min at room temperature, protected from light, and measured at 570 nm in a microplate reader. Values were normalized to cell number.

## **ANIMAL EXPERIMENTS**

All animal studies were approved by the Animal Care Committee of Wuhan University. USP30 KO mice were generated from the Model Animal Research Center, Nanjing University with CRISPR/Cas9 technology as a 64bp deletion in exon 4. For xenograft experiments, four-week-old male BALB/c nude mice were purchased from Model Animal Research Center (Nanjing, China) and maintained in microisolator cages. Detailed procedures were described previously.<sup>(30)</sup>

For the DEN/HFD-induced HCC model, C57/B6 mice were intraperitoneally administrated 25 mg/kg of diethylnitrosamine (DEN) (Sigma) on Day 15 of life. After 8-12 weeks, mice were fed a high-fat diet (HFD) (60% fat in calories; Research Diets, #D12492, New Brunswick, NJ) for the desired periods of time until being sacrificed.

For the DEN/CCl<sub>4</sub>-induced HCC model, DEN injections were performed as described above and CCl<sub>4</sub> (Sigma) was then injected weekly for 12 weeks (n=10 per group). Concentrated adeno-associated virus 8 (AAV8) encoding USP30 phosphorylation mutants or ACLY mutants were delivered by tail vein injections. Mice were sacrificed for analysis at 30 weeks.

Drug treatment protocols included intraperitoneal injection with phosphate-buffered saline (control group), anti-PD-L1 antibody at dose of 10 mg/kg every two weeks for 12 weeks, ETC1002 (30mg/kg per two days for 12 weeks) or anti-PD-L1 (10 mg/kg) with ETC1002 (30mg/kg) together for 12 weeks.

## **HUMAN HCC SAMPLES**

HCC samples were used as previously described.<sup>(29)</sup> Written-informed consent was obtained at the Union Hospital in Wuhan, China. The diagnoses of all samples were confirmed by histological review.

---

## Results

### USP30 DEFICIENCY ATTENUATES LIPOGENESIS AND TUMORIGENESIS

To identify the candidate deubiquitinases (deUbs) that participate in DEN-induced HCC development in mice maintained on normal control diets (NCDs) or HFDs, we analyzed the expression of 74 deUbs by qRT-PCR in liver and tumor tissues. Surprisingly, USP30 was the most up-regulated of all deUbs in the HFD-fed mice treated with DEN (Fig. 1A). USP7, USP21 and CYLD were also highly expressed and USP10 was repressed by DEN treatment as reported.<sup>(32-35)</sup> Western blot confirmed that USP30 protein was highly expressed in HFD-fed mice treated with DEN (Supporting Fig. S1A).

Usp30 Knockout (KO) mice (Supporting Fig. S1B, C) were then used to study the role of endogenous USP30 *in vivo* tumorigenesis. After confirming the absence of USP30 protein expression in their livers (Supporting Fig. S1D), WT and KO mice were placed on NCD and HFD with concurrent DEN treatment. Relative to WT mice, Usp30 KO mice had fewer tumor nodules and reduced tumor burden (Fig. 1B, C and Supporting Fig. S1E-G). DEN/HFD mice showed the severe lesion in Hematoxylin and eosin (H&E) staining, enhanced tumor with Ki67 and lipogenesis in Oil Red O staining compared with DEN-induced mice (Fig. 1D). Usp30 KO mice reduced the tissue lesion and lipogenesis in both NCD and HFD-fed mice (Fig. 1D).

Using tumor hepatocytes from DEN-induced HCC of KO and WT mice, we analyzed extracellular acidification rates (ECAR) and oxygen consumption rates (OCR) levels. Relative to WT cells, KO HCC cells showed reduced ECAR and OCR levels that were modestly increased by HFDs (Fig. 1E). These results indicated that USP30 promotes mitochondrial function by sustaining tumor metabolism especially in HFD diet in DEN-induced HCC.

Lipid enrichment analyses revealed that WT+HFD HCC contained larger amounts of free fatty acids (FFA), TGs and other lipids than Usp30 KO tumors (Fig. 1F). HCC from NCD Usp30 KO also contained lower levels of ATP and increased ROS (Supporting Fig. S1H-K). DEN/HFD WT tumors also contained higher levels of FFA, TG, FA and ATP and lower ROS levels compared

---

with DEN-WT and Usp30 KO mice (Fig. 1F and Supporting Fig. S1H-K).

Obesity has been associated with IL-6- and TNF $\alpha$ -induced inflammation.<sup>(6)</sup> ELISA and qRT-PCR indicated that Usp30 KO serum and tumors contained lower levels of TNF $\alpha$ , IL-6 and IL-1 $\beta$  (Fig. 1G-J and Supporting Fig. S1L-N). Thus the reduced overall lipid metabolism and inflammation of Usp30 KO tumors were associated with retarded liver tumor growth in both NCD and HFD mice.

### **IKK $\beta$ PHOSPHORYLATES AND STABILIZES USP30**

To investigate the function of USP30 in liver tumorigenesis, SDS-PAGE and Mass Spectrometry (MS) were conducted following ectopic expression of Flag-USP30 and immunoprecipitation. Interestingly, we discovered that several proteins related to lipogenesis such as ACLY and FASN and the NF- $\kappa$ B pathway members IKK $\beta$  and IKK $\alpha$  were co-purified with Flag-USP30 (Fig. 2A and Supporting Fig. S2A). As IKK $\beta$  was more abundant than IKK $\alpha$  in immuno-precipitates, we focused on our study on the former protein.

To verify the interaction between USP30 and IKK $\beta$ , endogenous co-immunoprecipitation (co-IP) experiments were conducted in HepG2 and Hep3B cell lines (Fig. 2B and Supporting Fig. S2B). Interaction with IKK $\beta$  truncation mutations indicated the N-terminal Kinase Domain (KD) to be responsible for the interaction (Fig. 2C). IP assay indicated that USP30 could be phosphorylated on serine sites by IKK $\beta$  (Supporting Fig. S2C). IKK $\beta$  overexpression promoted USP30 phosphorylation that was further increased by a constitutively active (CA) IKK $\beta$  construct rather than a kinase dead IKK $\beta$  (KD) mutant (Fig. 2D). The lack of USP30 phosphorylation by the IKK $\beta$  knock down was rescued by IKK $\beta$  (CA) mutant overexpression but not by the IKK $\beta$  (KD) mutant (Fig. 2E and Supporting Fig. S2D). SC-514, a selective IKK $\beta$  inhibitor, inhibits NF- $\kappa$ B-dependent gene expression in IL-1 $\beta$  stimulated synovial fibroblasts.<sup>(36)</sup> Serine phosphorylation of USP30 was abrogated in the presence of SC-514 (Supporting Fig. S2E).

Next we sought to identify the IKK $\beta$  phosphorylation sites on USP30. We searched for the predicted sites and mutated the two most likely of these, S210A and S364A. We determined that each one alone decreased the USP30 phosphorylation, and the effect was most pronounced when

---

the two mutations were combined (Fig. 2F). Moreover, the double S210/S364A mutation abolished its serine phosphorylation (Fig. 2G).

We next sought to determine whether IKK $\beta$ -mediated USP30 phosphorylation influenced its stabilization. ShRNA-mediated IKK $\beta$  inhibition reduced USP30 protein expression without affecting its mRNA levels (Supporting Fig. S2F, G) and this was rescued by the IKK $\beta$  CA but not the KD mutant (Fig. 2E and Supporting Fig. S2D). Following cycloheximide (CHX) chase, we found that IKK $\beta$  suppression shortened USP30 half-life whereas IKK $\beta$  overexpression extended it (Fig. 2H and Supporting Fig. S2H). Conversely, a USP30 phosphorylation dead mutant (S210/364A, 2SA) was destabilized while the S210/364D (2SD) mutant was stabilized (Fig. 2I). The similar results were found following overexpression of USP30 phosphorylation site mutants in Usp30 knockout MEF cells (Supporting Fig. S2I).

To investigate the role of USP30 phosphorylation in tumorigenesis, we stably expressed USP30 WT, 2SA and 2SD mutants in USP30 knockout HepG2 and Hep3B cells that were generated with CRISPR/Cas9 technology. These cell lines were then injected subcutaneously into nude mice and tumor xenografts were examined 35 days later. Western blot analysis confirmed the expression of each mutant (Supporting Fig. S3A). USP30 (2SD) promoted xenograft growth while USP30 (2SA) almost had no effect (Supporting Fig. S3B-D).

We next examined the consequences of each USP30 mutant on lipid metabolism. The USP30 phosphorylation mimetic 2SD but not 2SA increased lipogenesis, fatty acids (FA) and Triglyceride (TG) levels (Supporting Fig. S3E-G). Meanwhile, we found increased levels ATP in USP30 (2SD) tumors rather than 2SA mutant (Supporting Fig. S3H), suggesting that these were needed to support more rapid tumor growth.

### **USP30 DEUBIQUITINATES AND STABILIZES ACLY AND FASN**

IP indicated that USP30 interacted with both ACLY and FASN (Fig. 3A and Supporting Fig. S4A), and domain mapping demonstrated that the CoA ligase domain of ACLY and the Enoyl reductase domain of FASN interacted with USP30 (Supporting Fig. S4B, C). Previous data reveal that the ACLY and FASN protein levels dramatically decrease in Usp30 knockout mouse liver

---

cancer (Fig. 1C). Next, we check whether USP30 regulates ACLY and FASN protein stability in liver cancer cells. The result showed that shRNA-mediated USP30 inhibition reduced ACLY and FASN protein levels in HepG2 and Hep3B cells and this was rescued by the USP30 WT protein but not the catalytically inactive mutant (C77S) (Fig. 3B). Moreover, USP30 depletion repressed ACLY activity and this was rescued by WT USP30 but not by USP30 (C77S) overexpression (Fig. 3C). USP30 phosphorylation mutants largely abrogated the interaction between USP30 and ACLY or FASN (Fig. 3D and Supporting Fig. S4D). CHX chase studies indicated that USP30 inhibition attenuated ACLY and FASN half-life, while USP30 overexpression promoted ACLY and FASN stabilization (Fig. 3E and Supporting Fig. S4E, F). Moreover, we found that the proteasome inhibitor MG132 largely stabilized ACLY and FASN rather than  $\text{NH}_4\text{Cl}$  or 3-MA (Fig. 3F).

We next asked whether USP30 stabilized ACLY and FASN by altering their ubiquitination status. IP experiments indicated that WT USP30 but not USP30 C77S decreased ACLY ubiquitination (Fig. 3G) and that USP30 inhibition increased ACLY ubiquitination (Supporting Fig. S5A). More specifically, USP30 inhibited K48-linked ubiquitination of ACLY (Fig. 3H). In turn, only K48R-linked ubiquitin had no effect on ACLY ubiquitination (Supporting Fig. S5B), suggesting that USP30 deubiquitinated ACLY mainly through K48. Using predicted ubiquitination sites as a guide, we discovered that USP30 deubiquitinated ACLY on K540, K546 and K554 (Fig. 3I). IKK $\beta$  overexpression inhibited ACLY ubiquitination whereas the reverse was true when IKK $\beta$  was inhibited (Supporting Fig. S5C, D). Consistent with this, the USP30 phosphorylation inactive mutant 2SA promoted ACLY ubiquitination whereas the phosphorylation mimic 2SD mutant had the opposite effect (Fig. 3J).

CUL3, a core component of the cullin-RING-based BCR (BTB-CUL3-RBX1) E3 ubiquitin-protein ligase complex, has been reported to promote ACLY ubiquitination. We therefore explored whether this activity might proceed via USP30. Indeed, ectopic USP30 expression repressed CUL3-mediated ACLY ubiquitination, whereas USP30 depletion rescued the reduction in ubiquitination caused by CUL3 inhibition (Fig. 3K and Supporting Fig. S5E). Thus the deubiquitination of ACLY appears to proceed via the BCR E3 ubiquitin-protein ligase complex.

---

WT USP30 but not its C77S mutant also deubiquitinated FASN whereas USP30 inhibition facilitated this (Supporting Fig. S5F, G). FASN modification appeared to proceed mainly through K6O- and K48O-linked ubiquitin and K6/48R-linked ubiquitin abrogated FASN ubiquitination (Supporting Fig. S5H, I). Taken together, these results indicate that USP30 stabilizes ACLY and FASN through K48 and K6/48-linked deubiquitination respectively.

### **ACLY MEDIATES USP30'S ENHANCEMENT OF THE ONCOGENIC PHENOTYPES**

To investigate whether USP30-mediated tumorigenesis was dependent on ACLY, we overexpressed USP30 and then inhibited ACLY in HepG2 and Hep3B cells. Xenograft experiment showed that USP30 overexpression and ACLY depletion respectively enhanced and reduced tumorigenesis (Supporting Fig. S6A-C) and that ACLY inhibition countered the effects of USP30 overexpression (Supporting Fig. S6A-C).

Ectopic USP30 expression promoted the accumulation of TGs and fatty acids in tumors, enhanced lipogenesis, ACLY activity and increased tumor ATP levels (Supporting Fig. S6D-H). USP30 overexpression as well as ACLY inhibition moderately reduced the TG, FA levels, lipogenesis, ACLY activity and ATP levels (Supporting Fig. S6D-H).

In contrast to the findings made in tumors overexpressing USP30, its depletion inhibited tumor growth in a manner that was rescued by ACLY overexpression (Supporting Fig. S7A-C). Moreover, the effects on metabolic parameters were the opposite of those seen in response to USP30 overexpression (Supporting Fig. S7D-H). Collectively, these and the foregoing findings indicated that the tumor-altering properties of USP30 were mediated at least in part by ACLY.

### **IKK $\beta$ PHOSPHORYLATES AND STABILIZES ACLY**

Further investigation of the consequences of the IKK $\beta$ -ACLY interaction indicated that IKK $\beta$  promoted ACLY serine phosphorylation and that IKK $\beta$  inhibition had the opposite effect (Fig. 4A-E and Supporting Fig. S8A). Additionally, IKK $\beta$  depletion suppressed ACLY protein levels and activity, while the IKK $\beta$  CA but not the KD mutant overexpression rescued these defects in

---

both HepG2 and Hep3B cells (Fig. 4F and Supporting Fig. S8B). Both ACLY phosphorylation and expression were responsive to IKK $\beta$  inhibitor in a dose-dependent manner (Supporting Fig. S8C).

ACLY S451, S455 and S457 were all determined to be sites of phosphorylation for IKK $\beta$  (Fig. 4G). This was further supported by the fact that three point mutations in these residues completely abrogated IKK $\beta$ -mediated ACLY phosphorylation (Supporting Fig. S8D-F). We then found that ACLY S451/455/457A (3SA) triple failed to interact with USP30 whereas the ACLY S451/455/457D (3SD) mutant enhanced the interaction (Fig. 4H). The ACLY phosphorylation-inactive mutant 3SA also facilitated ACLY ubiquitination whereas the active mutant 3SD repressed ACLY ubiquitination (Fig. 4I and Supporting Fig. S8G). USP30 repression further increased ACLY ubiquitination (Supporting Fig. S8H). IKK $\beta$  inhibition also reduced ACLY's half-life and IKK $\beta$  repressed ACLY degradation through the proteasome pathway (Fig. 4J and Supporting Fig. S8I). Finally, the IKK $\beta$  inhibitor SC-514 promoted rapid ACLY degradation in both HepG2 and Hep3B cells (Fig. 4K). Collectively, these findings establish that, in addition to its effects on USP30, IKK $\beta$  directly phosphorylates ACLY at multiple sites and stabilizes the latter protein.

### **USP30 AND ACLY PHOSPHORYLATION PROMOTE TUMOR GROWTH IN DEN/CCL<sub>4</sub> INDUCED HCC**

To determine whether USP30 and ACLY phosphorylation influenced tumor growth, adeno-associated virus 8 (AAV8) expressing USP30 or the USP30 phosphorylation mutant (2SA/2SD, S210/364A/D) was administered to DEN/CCL<sub>4</sub>-treated mice and tumor burdens were assessed at week 30. Western blots showed the expression of each protein in different tumors (Fig. 5A). Tumors from Usp30 KO as well as USP30 (2SA) overexpression were smaller and contained fewer nodules, whereas the reverse was true for USP30 WT and 2SD overexpression in Usp30 KO mice (Fig. 5B-F). USP30 WT and 2SD mice also contained higher levels of FFAs, TGs, lipid synthesis and ATP (Fig. 5G-I). Conversely, USP30 WT and 2SD overexpression showed lower levels of ROS (Fig. 5J). Usp30 KO tumors also contained lower levels of TNF $\alpha$ , IL-6 and IL-1 $\beta$

---

relative to USP30 WT and 2SD HCCs (Fig. 5K-M).

Our data also show that the ACLY phosphorylation and total protein also dramatically increased in DEN and HFD induced HCC compared with normal liver in mice (Supporting Fig. S1A). Therefore, we also overexpressed the ACLY WT and ACLY phosphorylation mutant (3SA/3SD, S451/455/457 A/D) in *Usp30* KO mice (Supporting Fig. S9A, B). H&E and Ki-67 staining revealed more severe liver damage and proliferation in ACLY WT and 3SD overexpression livers (Supporting Fig. S9C). ACLY WT and 3SD were associated with increased nodule numbers, volumes, liver weights, FFAs, TGs, ATP levels and reduced ROS levels (Supporting Fig. S9G-J). ACLY 3SA had no obvious effect on nodule numbers, volumes, tumor weights, and their above biochemical parameters (Supporting Fig. S9B-J). Additionally, tumors with ACLY WT and 3SD overexpression were associated with high cytokine levels (Supporting Fig. S9K-M). Collectively, these findings indicate that IKK $\beta$ -mediated ACLY phosphorylation promoted lipogenesis, inflammation and tumor growth.

#### **SUPPRESSION OF DEN/CCL<sub>4</sub> HEPATOCARCINOGENESIS BY THE TARGETING OF ACLY AND PD-L1**

ETC1002, an ACLY inhibitor and adenosine monophosphate-activated protein kinase (AMPK) activator, is a promising therapeutic strategy to lower LDL-C levels in hypercholesterolemic patients.<sup>(37)</sup> PD-L1 is transcriptionally activated by NF- $\kappa$ B and expressed at high levels in many HCCs.<sup>(38)</sup> We therefore determined the efficacy of targeting ACLY and PD-L1 with ETC1002 and anti-PD-L1, respectively. Surprisingly, this combination markedly inhibited DEN/HFD induced HCC (Fig. 6A). Staining with H&E, Ki-67 and Oil Red O and assessments of other biological and biochemical parameters showed modest effects of ETC1002 when administered individually but marked synergy when combination with anti-PD-L1 (Fig. 6B-L). Similar findings were made in mice that had been maintained on DEN/CCL<sub>4</sub>'s (Supporting Fig. S10A-L). Thus combination therapy with an ACLY inhibitor and anti-PD-L1 markedly suppressed DEN/HFD and DEN/CCL<sub>4</sub>-induced HCC.

#### **THE IKKB-USP30-ACLY AXIS IS UPREGULATED IN HUMAN HCCS**

---

We analyzed the TCGA and Human Protein Atlas databases and found that USP30 levels were elevated in a variety of tumor subsets (Supporting Fig. S11A, B). Previous data show that USP30, IKK $\beta$ , P-ACLY, ACLY and FASN were robustly increased in DEN/HFD induced mouse liver cancer compared with normal liver (Supporting Fig. S1A). Western blotting verified the upregulation of IKK $\beta$ , P-Ser USP30, USP30, P-ACLY, ACLY and FASN in human HCC patient samples (Fig. 7A, B and Supporting Fig. S11C, D). The metabolic levels of fatty acids were also upregulated in the tumor patients compared with adjacent normal tissues (Fig. 7C). Also the IKK $\beta$  levels were positive correlated with the levels of USP30, ACLY, P-ACLY, FASN, and the USP30 levels were positive correlated with the levels of ACLY, P-ACLY and FASN (Fig. 7D, E and Supporting Fig. S11E-G). Moreover, the expression of IKK $\beta$  and USP30 were positive correlated with fatty acids levels (Fig. 7F, G). Altogether, these findings indicate that up-regulation of the IKK $\beta$ -USP30-ACLY axis in experimental murine HCCs extended to human HCCs and certain other cancers as well.

---

## Discussion

Cancer cells often show dysregulated lipid metabolism and inflammation.<sup>(3)</sup> Intracellular FAs serve as biosynthetic precursors of membrane lipids, signaling molecules and modifying groups and provide an alternate energy storage for tumor growth.<sup>(39)</sup> In this work, we discovered that IKK $\beta$  phosphorylates USP30 and ACLY, which in turn promotes ACLY deubiquitination. In the absence of USP30, lipid synthesis, inflammation and hepatocarcinogenesis are markedly inhibited. The simultaneous inhibition of ACLY and PD-L1, the latter of which is upregulated by IKK $\beta$  as well, dramatically suppresses hepatocarcinogenesis (Fig. 7J). Together, these findings identify a previously unappreciated set of relationships, i.e. the IKK $\beta$ -USP30-ACLY axis, that play important roles in lipid metabolism, inflammation and tumorigenesis. These also provide reason to believe and targeting this pathway could provide a novel therapeutic approach for HCC and possibly other cancers as well.

IKK $\beta$  has been demonstrated to promote HCC progression with or without NF- $\kappa$ B activation. It was reported that CPAP is essential for the interaction between IKK $\beta$  and NF- $\kappa$ B. SUMOylated CPAP enhances HBX-induced NF- $\kappa$ B activation and HCC development.<sup>(40)</sup> Inactivation of the BH3-only protein BAD by IKK $\beta$  independently of NF- $\kappa$ B activation suppresses TNF- $\alpha$  induced apoptosis.<sup>(41)</sup> IKK $\alpha$  and IKK $\beta$  directly phosphorylate RIPK1 to regulate hepatocarcinogenesis and cholestasis.<sup>(42)</sup> In our study, we identified that IKK $\beta$  directly phosphorylated USP30 and stabilized USP30, which promoted USP30 deubiquitination and HCC development.

Moreover, we demonstrated that IKK $\beta$  also phosphorylated ACLY and enhanced its deubiquitination, lipid metabolism and inflammation. We discovered IKK $\beta$ -mediated phosphorylation of USP30 decreased ROS production. ROS are involved in physiological processes as a messenger in cellular signaling. Many studies have shown the tumor repressing properties of endogenous and exogenous antioxidants.<sup>(43)</sup> ACLY inhibition has showed an anticancer effect via increased ROS and AMPK phosphorylation.<sup>(44)</sup> In our study, the increased ROS production and reduced ATP in DEN-induced HCC from USP30 KO mice may due to the ACLY deficiency, thus preventing HCC development.

---

Under inflammation conditions, cells have an acute need to generate sufficient energy and biomolecules to support growth and proliferation. TLR4 and IKK $\beta$  dependent inflammatory events were required for saturated fatty acid-induced ceramide biosynthesis in response to obesity.<sup>(45)</sup> In this work, we suggested that IKK $\beta$ -induced inflammation activation may promote lipid synthesis through ACLY phosphorylation and then promote HCC. Conversely, lipid metabolism can also affect inflammation, tumor microenvironment and then hepatocarcinogenesis. ACLY depletion compromised IL-2-mediated CD4<sup>+</sup> T lymphocytes growth.<sup>(46)</sup> Recently, Karin's group discovered that inhibition of CTL1 expression or choline phosphorylation attenuated NLRP3 inflammasome activation and IL-1 $\beta$ , IL-18 production in stimulated macrophages.<sup>(47)</sup> In our work, IKK $\beta$ -mediated ACLY phosphorylation induces lipogenesis and promotes production of inflammatory cytokines such as TNF- $\alpha$ , IL-6 and IL-1 $\beta$ , indicating the reciprocal links between inflammation, lipid metabolism and tumorigenesis.

Combination therapy is currently emerging as a promising treatment. Targeting inflammation and lipid metabolism might be a new potential therapy in HCC treatment. Programmed cell death-ligand 1 (PD-L1) is known to be transcriptionally activated by NF- $\kappa$ B in various cancer types.<sup>(38)</sup> PD-L1 generates an immunosuppressive tumor microenvironment by suppressing T cell activation and allowing the expansion of otherwise immuno-reactive tumor cells.<sup>(48)</sup> In HCC patients, increased PD-L1 expression is associated with tumor aggressiveness, macrovascular invasion and poor differentiation.<sup>(49)</sup> In the current study, we found there to be only a modest effect of anti-PD-L1 inhibition on HCC development. However, in combination with bempedoic acid (ETC1002), dramatic synergy was attained. ETC1002 is a novel ACLY inhibitor that is currently being evaluated in phase 3 clinical trials as a cholesterol-reducing agent.<sup>(50)</sup>

In summary, we identified a new IKK $\beta$ -USP30-ACLY axis that plays an essential role in the lipogenesis and liver cancer. USP30 deficiency largely abrogated lipid metabolism, inflammation and DEN/HFD-induced HCC. And targeting ACLY as well as PD-L1 offers a new possibility for HCC therapy.

---

## **Acknowledgements**

We thank Profs. Qunying Lei (Fudan University, Shanghai) for the ACLY and FASN vectors, Yan Wang (Wuhan University, Wuhan, China) for the AAV8 vector and Jinxiang Zhang (Wuhan Union Hospital, Wuhan, China) for providing the HCC samples.

---

## REFERENCES

- 1) Marquardt JU, Thorgeirsson SS. SnapShot: Hepatocellular carcinoma. *Cancer Cell* 2014;25:550 e551.
- 2) Thorgeirsson SS, Grisham JW. Molecular pathogenesis of human hepatocellular carcinoma. *Nat Genet* 2002;31:339-346.
- 3) Currie E, Schulze A, Zechner R, Walther TC, Farese RV, Jr. Cellular fatty acid metabolism and cancer. *Cell Metab* 2013;18:153-161.
- 4) Menendez JA, Lupu R. Fatty acid synthase and the lipogenic phenotype in cancer pathogenesis. *Nat Rev Cancer* 2007;7:763-777.
- 5) Guri Y, Colombi M, Dazert E, Hindupur SK, Roszik J, Moes S, et al. mTORC2 Promotes Tumorigenesis via Lipid Synthesis. *Cancer Cell* 2017;32:807-823 e812.
- 6) Park EJ, Lee JH, Yu GY, He G, Ali SR, Holzer RG, et al. Dietary and genetic obesity promote liver inflammation and tumorigenesis by enhancing IL-6 and TNF expression. *Cell* 2010;140:197-208.
- 7) Taniguchi K, Karin M. NF-kappaB, inflammation, immunity and cancer: coming of age. *Nat Rev Immunol* 2018;18:309-324.
- 8) Bingol B, Tea JS, Phu L, Reichelt M, Bakalarski CE, Song Q, et al. The mitochondrial deubiquitinase USP30 opposes parkin-mediated mitophagy. *Nature* 2014;510:370-375.
- 9) Liang JR, Martinez A, Lane JD, Mayor U, Clague MJ, Urbe S. USP30 deubiquitylates mitochondrial Parkin substrates and restricts apoptotic cell death. *EMBO Rep* 2015;16:618-627.
- 10) Yue W, Chen Z, Liu H, Yan C, Chen M, Feng D, et al. A small natural molecule promotes mitochondrial fusion through inhibition of the deubiquitinase USP30. *Cell Res* 2014;24:482-496.
- 11) Cunningham CN, Baughman JM, Phu L, Tea JS, Yu C, Coons M, et al. USP30 and parkin homeostatically regulate atypical ubiquitin chains on mitochondria. *Nat Cell Biol* 2015;17:160-169.
- 12) Gersch M, Gladkova C, Schubert AF, Michel MA, Maslen S, Komander D. Mechanism and regulation of the Lys6-selective deubiquitinase USP30. *Nat Struct Mol Biol* 2017;24:920-930.
- 13) DiDonato JA, Mercurio F, Karin M. NF-kappaB and the link between inflammation and cancer. *Immunol Rev* 2012;246:379-400.
- 14) Mercurio F, Zhu H, Murray BW, Shevchenko A, Bennett BL, Li J, et al. IKK-1 and IKK-2: cytokine-activated IkkappaB kinases essential for NF-kappaB activation. *Science* 1997;278:860-866.
- 15) Kawauchi K, Araki K, Tobiume K, Tanaka N. p53 regulates glucose metabolism through an IKK-NF-kappaB pathway and inhibits cell transformation. *Nat Cell Biol* 2008;10:611-618.

- 
- 16) Heuser C, Gotot J, Piotrowski EC, Philipp MS, Courreges CJF, Otte MS, et al. Prolonged IKKbeta Inhibition Improves Ongoing CTL Antitumor Responses by Incapacitating Regulatory T Cells. *Cell Rep* 2017;21:578-586.
- 17) Hu MC, Lee DF, Xia W, Golfman LS, Ou-Yang F, Yang JY, et al. IkappaB kinase promotes tumorigenesis through inhibition of forkhead FOXO3a. *Cell* 2004;117:225-237.
- 18) Lee DF, Kuo HP, Chen CT, Hsu JM, Chou CK, Wei Y, et al. IKK beta suppression of TSC1 links inflammation and tumor angiogenesis via the mTOR pathway. *Cell* 2007;130:440-455.
- 19) Maeda S, Kamata H, Luo JL, Leffert H, Karin M. IKKbeta couples hepatocyte death to cytokine-driven compensatory proliferation that promotes chemical hepatocarcinogenesis. *Cell* 2005;121:977-990.
- 20) Burke AC, Huff MW. ATP-citrate lyase: genetics, molecular biology and therapeutic target for dyslipidemia. *Curr Opin Lipidol* 2017;28:193-200.
- 21) Bauer DE, Hatzivassiliou G, Zhao F, Andreadis C, Thompson CB. ATP citrate lyase is an important component of cell growth and transformation. *Oncogene* 2005;24:6314-6322.
- 22) Zaidi N, Swinnen JV, Smans K. ATP-citrate lyase: a key player in cancer metabolism. *Cancer Res* 2012;72:3709-3714.
- 23) Beigneux AP, Kosinski C, Gavino B, Horton JD, Skarnes WC, Young SG. ATP-citrate lyase deficiency in the mouse. *J Biol Chem* 2004;279:9557-9564.
- 24) Sato R, Okamoto A, Inoue J, Miyamoto W, Sakai Y, Emoto N, et al. Transcriptional regulation of the ATP citrate-lyase gene by sterol regulatory element-binding proteins. *J Biol Chem* 2000;275:12497-12502.
- 25) Migita T, Narita T, Nomura K, Miyagi E, Inazuka F, Matsuura M, et al. ATP citrate lyase: activation and therapeutic implications in non-small cell lung cancer. *Cancer Res* 2008;68:8547-8554.
- 26) Lucenay KS, Doostan I, Karakas C, Bui T, Ding Z, Mills GB, et al. Cyclin E Associates with the Lipogenic Enzyme ATP-Citrate Lyase to Enable Malignant Growth of Breast Cancer Cells. *Cancer Res* 2016;76:2406-2418.
- 27) Lin R, Tao R, Gao X, Li T, Zhou X, Guan KL, et al. Acetylation stabilizes ATP-citrate lyase to promote lipid biosynthesis and tumor growth. *Mol Cell* 2013;51:506-518.
- 28) Zhang C, Liu J, Huang G, Zhao Y, Yue X, Wu H, et al. Cullin3-KLHL25 ubiquitin ligase targets ACLY for degradation to inhibit lipid synthesis and tumor progression. *Genes Dev* 2016;30:1956-1970.
- 29) Han H, Sun D, Li W, Shen H, Zhu Y, Li C, et al. A c-Myc-MicroRNA functional feedback loop affects hepatocarcinogenesis. *Hepatology* 2013;57:2378-2389.
- 30) Gu L, Zhu Y, Lin X, Li Y, Cui K, Prochownik EV, et al. Amplification of Glyceronephosphate O-Acyltransferase and

- 
- Recruitment of USP30 Stabilize DRP1 to Promote Hepatocarcinogenesis. *Cancer Res* 2018;78:5808-5819.
- 31) Jackson LE, Kulkarni S, Wang H, Lu J, Dolezal JM, Bharathi SS, et al. Genetic Dissociation of Glycolysis and the TCA Cycle Affects Neither Normal nor Neoplastic Proliferation. *Cancer Res* 2017;77:5795-5807.
- 32) Cai JB, Shi GM, Dong ZR, Ke AW, Ma HH, Gao Q, et al. Ubiquitin-specific protease 7 accelerates p14(ARF) degradation by deubiquitinating thyroid hormone receptor-interacting protein 12 and promotes hepatocellular carcinoma progression. *Hepatology* 2015;61:1603-1614.
- 33) Li W, Cui K, Prochownik EV, Li Y. The deubiquitinase USP21 stabilizes MEK2 to promote tumor growth. *Cell Death Dis* 2018;9:482.
- 34) Welte S, Urbanik T, Ellsner C, Kautz N, Koehler BC, Waldburger N, et al. Nuclear expression of the deubiquitinase CYLD is associated with improved survival in human hepatocellular carcinoma. *PLoS One* 2014;9:e110591.
- 35) Lu C, Ning Z, Wang A, Chen D, Liu X, Xia T, et al. USP10 suppresses tumor progression by inhibiting mTOR activation in hepatocellular carcinoma. *Cancer Lett* 2018;436:139-148.
- 36) Kishore N, Sommers C, Mathialagan S, Guzova J, Yao M, Hauser S, et al. A selective IKK-2 inhibitor blocks NF-kappa B-dependent gene expression in interleukin-1 beta-stimulated synovial fibroblasts. *J Biol Chem* 2003;278:32861-32871.
- 37) Filippov S, Pinkosky SL, Newton RS. LDL-cholesterol reduction in patients with hypercholesterolemia by modulation of adenosine triphosphate-citrate lyase and adenosine monophosphate-activated protein kinase. *Curr Opin Lipidol* 2014;25:309-315.
- 38) Jin X, Ding D, Yan Y, Li H, Wang B, Ma L, et al. Phosphorylated RB Promotes Cancer Immunity by Inhibiting NF-kappaB Activation and PD-L1 Expression. *Mol Cell* 2019;73:22-35 e26.
- 39) Maan M, Peters JM, Dutta M, Patterson AD. Lipid metabolism and lipophagy in cancer. *Biochem Biophys Res Commun* 2018;504:582-589.
- 40) Yang ST, Yen CJ, Lai CH, Lin YJ, Chang KC, Lee JC, et al. SUMOylated CPAP is required for IKK-mediated NF-kappaB activation and enhances HBx-induced NF-kappaB signaling in HCC. *J Hepatol* 2013;58:1157-1164.
- 41) Yan J, Xiang J, Lin Y, Ma J, Zhang J, Zhang H, et al. Inactivation of BAD by IKK inhibits TNFalpha-induced apoptosis independently of NF-kappaB activation. *Cell* 2013;152:304-315.
- 42) Koppe C, Verheugd P, Gautheron J, Reisinger F, Kreggenwinkel K, Roderburg C, et al. IkappaB kinasealpha/beta control biliary homeostasis and hepatocarcinogenesis in mice by phosphorylating the cell-death mediator receptor-interacting protein kinase 1. *Hepatology* 2016;64:1217-1231.

- 
- Accepted Article
- 43) Sabharwal SS, Schumacker PT. Mitochondrial ROS in cancer: initiators, amplifiers or an Achilles' heel? *Nat Rev Cancer* 2014;14:709-721.
  - 44) Migita T, Okabe S, Ikeda K, Igarashi S, Sugawara S, Tomida A, et al. Inhibition of ATP citrate lyase induces an anticancer effect via reactive oxygen species: AMPK as a predictive biomarker for therapeutic impact. *Am J Pathol* 2013;182:1800-1810.
  - 45) Holland WL, Bikman BT, Wang LP, Yuguang G, Sargent KM, Bulchand S, et al. Lipid-induced insulin resistance mediated by the proinflammatory receptor TLR4 requires saturated fatty acid-induced ceramide biosynthesis in mice. *J Clin Invest* 2011;121:1858-1870.
  - 46) Osinalde N, Mitxelena J, Sanchez-Quiles V, Akimov V, Aloria K, Arizmendi JM, et al. Nuclear Phosphoproteomic Screen Uncovers ACLY as Mediator of IL-2-induced Proliferation of CD4+ T lymphocytes. *Mol Cell Proteomics* 2016;15:2076-2092.
  - 47) Sanchez-Lopez E, Zhong Z, Stubelius A, Sweeney SR, Booshehri LM, Antonucci L, et al. Choline Uptake and Metabolism Modulate Macrophage IL-1beta and IL-18 Production. *Cell Metab* 2019;29:1350-1362 e1357.
  - 48) Pardoll DM. The blockade of immune checkpoints in cancer immunotherapy. *Nat Rev Cancer* 2012;12:252-264.
  - 49) Gao Q, Wang XY, Qiu SJ, Yamato I, Sho M, Nakajima Y, et al. Overexpression of PD-L1 significantly associates with tumor aggressiveness and postoperative recurrence in human hepatocellular carcinoma. *Clin Cancer Res* 2009;15:971-979.
  - 50) Ruscica M, Banach M, Sahebkar A, Corsini A, Sirtori CR. ETC-1002 (Bempedoic acid) for the management of hyperlipidemia: from preclinical studies to phase 3 trials. *Expert Opin Pharmacother* 2019;20:791-803.

## Figure Legends

**Fig. 1.** Usp30 deficiency attenuates lipogenesis and tumorigenesis. (A) Heatmap showing mRNA expression levels of 74 deubiquitinases in the livers of NCD- and HFD-fed mice treated with DEN (n=5). (B) Typical appearance of livers from the indicated mice. DEN (25 mg/ml) was injected 15 days after birth (n=10). After 12 weeks, mice were provided with HFDs or NCDs for the desired periods of time until being sacrificed. (C) Expression of the indicated proteins from the livers described in (B). (D) Representative images of tumor sections stained for H&E, Ki-67 and ORO. Scale bars, 50  $\mu$ m. (E) ECAR and OCR analyses of primary hepatocytes from 8-week-old Usp30 KO or WT mice. (F) Summary of all significantly different lipid metabolites from WT, Usp30 KO, WT+HFD and Usp30 KO+HFD mice. FFA, free fatty acids; PA, phosphatidic acids; PC, phosphatidylcholines; PE, phosphatidyl ethanolamines; LPE, lyso-PE; PG, phosphatidyl glycerols; PI, phosphatidylinositols; PS, phosphatidylserines; CAR, carnitine; DG, diacylglycerols; LPC, lyso-PC; PC-O, alkylphosphatidylcholine; Cer, Ceramide; SM, sphingomyelin; TG, triacylglycerols. (G-J) Serum and tumor levels of TNF $\alpha$  (G, H) and IL-6 (I, J) in mice from 1B. Data are presented as mean  $\pm$  SD. \*, P < 0.05; \*\*, P < 0.01; \*\*\*, P < 0.001.

**Fig. 2.** IKK $\beta$  phosphorylates and stabilizes USP30. (A) Scatterplots showing MS results of IPs from HEK293 cells expressing Flag-USP30 after subtracting background of mock-transfected cell IPs. (B) Endogenous interaction between IKK $\beta$  and USP30. Whole cell lysates from HepG2 and Hep3B cells were prepared and Co-IPs were performed with antibodies against the indicated proteins. IP and IB were performed using antibodies against USP30 and IKK $\beta$ . (C) Schematic diagram showed the structure of IKK $\beta$  (left) and the truncation mutants that were co-expressed with HA-USP30 in HEK293. Extracts were immunoprecipitated with Flag antibody and the precipitates were then probed with HA antibodies (right). (D) IKK $\beta$  and its constitutive activation (CA) mutant promote USP30 Serine phosphorylation. HEK293 cells were transfected with IKK $\beta$ , IKK $\beta$  (CA) or IKK $\beta$  (KD) and HA-USP30. IP and IB were performed with the indicated antibodies. (E) IKK $\beta$  (CA) but not KD promotes IKK $\beta$  phosphorylation and stabilization in

---

HepG2 cells. (F) IKK $\beta$  phosphorylates USP30 at S210 and S364. HEK293 cells were transfected with the indicated vectors. IP and IB were performed with indicated the antibodies. (G) IKK $\beta$  inhibitor (SC-514) affects the phosphorylation of USP30 WT and USP30 S210/364 mutant. IP and IB were performed with indicated the antibodies. (H) USP30 phosphorylation by IKK $\beta$  affects its turnover. HEK293 cells were transfected with the indicated vectors. Cells were treated with CHX (50  $\mu$ g/ml) for the indicated time and the expression of USP30 and IKK $\beta$  were the analyzed by western blotting (left). The intensity of USP30 expression for each time point was quantified by densitometry and normalized to the  $\beta$ -actin loading control (right). (I) USP30 phosphorylation prolongs its half-life. The intensity of USP30 expression for each time point was quantified by densitometry with  $\beta$ -actin as described in (I). Data are presented as mean  $\pm$  SD. \*, P < 0.05; \*\*, P < 0.01.

**Fig. 3.** USP30 deubiquitinates and stabilizes ACLY and FASN. (A) Endogenous interaction between ACLY and USP30 in HepG2 and Hep3B cells. Whole cell lysates were prepared and IPs were performed with antibodies against the indicated proteins. Immunocomplexes were then immuno-blotted using antibodies against ACLY and USP30. (B) Western blot assay of ACLY and FASN levels in USP30-depleted HepG2 and Hep3B cells. (C) ACLY activity of the cells from (B) were analyzed. (D) USP30 phosphorylation mutation abrogates its interaction with ACLY. (E) USP30 knockdown reduces the half-lives of ACLY and FASN. (F) USP30 inhibits ACLY and FASN degradation via the protease pathway. ACLY and FASN immunoblots of lysates from HEK293 cells transfected with shUSP30 after treatment with NH<sub>4</sub>Cl (25 mM), MG132 (100  $\mu$ M) or 3-MA (500 ng/ml) for 6 h. (G) WT USP30 but not its C77S mutant inhibits ACLY ubiquitination. (H) USP30 reduces the K48-linked ubiquitination of ACLY. (I) USP30 deubiquitinates ACLY at K540/546/554 sites. (J) The phosphorylation defective USP30 mutant promotes ACLY ubiquitination while the phospho-mimetic mutant USP30 S2D has the reverse effect. (K) USP30 reverses CUL3-mediated ACLY ubiquitination. (G-K) Expression of the indicated proteins following their transient over-expression in HEK293. MG132 (100  $\mu$ M) was added to the cells 6h before harvested. Then IPs and IBs were performed with the indicated

antibodies. Data are presented as mean  $\pm$  SD. \*,  $P < 0.05$ ; \*\*,  $P < 0.01$ .

**Fig. 4.** IKK $\beta$  phosphorylates and stabilizes ACLY. (A) Endogenous interaction between ACLY and IKK $\beta$  in HepG2 and Hep3B cells. (B and C) Exogenous interaction between ACLY and IKK $\beta$ . Flag-tagged ACLY or truncation mutants were co-expressed with HA-IKK $\beta$  (B). Flag-tagged WT IKK $\beta$  or the indicated truncation mutants were co-expressed with HA-ACLY in HEK293 (C). Extracts were immunoprecipitated with Flag antibody and examined by western blotting. (D) Pan phospho-serine levels of ACLY were upregulated in cells treated with phosphatase inhibitor cocktail. (E) IKK $\beta$  knockdown reduces serine phosphorylation of ACLY. (F) Western blot assay of ACLY phosphorylation and total protein levels in IKK $\beta$ -depleted HepG2 cells. (G) IKK $\beta$  phosphorylates ACLY at S451/455/457 sites. HEK293 were transfected with Flag-ACLY +/- HA-IKK $\beta$  and the indicated mutants. Total lysates were IP with Flag antibody and immune-blotted with the indicated antibodies. (H) ACLY 3SA depletes its interaction with USP30 while USP30 3SD enhances the interaction of ACLY and USP30. (I) HEK293 cells were transfected with Myc-Ub, HA-USP30 and Flag-ACLY (WT), or Flag-ACLY (3SA), Flag-ACLY (3SD) and treated with MG132 for 6h. Cell lysates were IP with Flag-beads and then IB with indicated antibodies. (J) CHX chase of ACLY protein level with or without shRNA-mediated IKK $\beta$  inhibition. The intensity of ACLY expression for each time point was quantified by densitometry using  $\beta$ -actin as a control for protein loading. The results of three identical experiments are shown in the graph. (K) HepG2 cells were treated with SC-514 (100  $\mu$ M) for 1 hour followed by CHX chase for the indicated times. Normalization was as described in (J). The results of three identical experiments are shown in the graph. Data were presented as mean  $\pm$  SD. \* $P < 0.05$ , \*\* $P < 0.01$ .

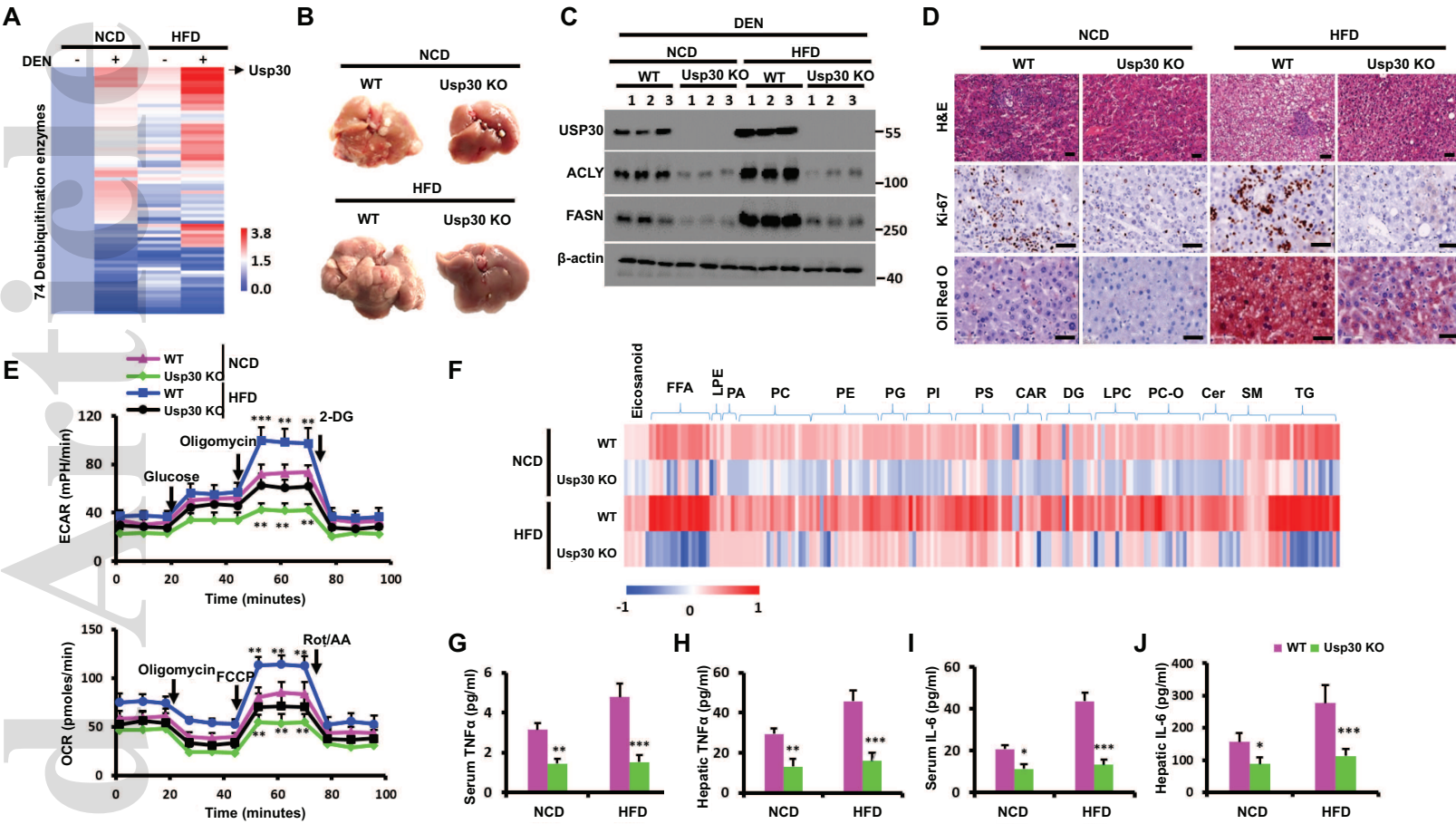
**Fig. 5.** USP30 phosphorylation promotes lipogenesis and tumorigenesis. (A) Western blot analysis of the indicated proteins following injection of AAV8-WT USP30 or AAV8-USP30 2SA or 2SD in DEN/CCl<sub>4</sub> induced Usp30 KO mouse HCCs. (B) Typical appearance of the HCCs arising in the livers described in (A). (C) Tumors from (B) stained with H&E or Ki-67. Scale bars, 50  $\mu$ m. (D-J) tumor nodule number (D), tumor volumes (E), Liver weights (F), fatty acids levels (G), TG levels

(H), ATP levels (I) and ROS levels (J) in the HCCs described in (A) and (B). (K) TNF $\alpha$ , IL-1 $\beta$ , and IL-6 transcript levels in mice from 5B. (L and M) The TNF $\alpha$  and IL-6 levels of serum (L) and liver (M) from Figure 5B. Data are presented as mean  $\pm$  SD. \*P, < 0.05; \*\*, P < 0.01; \*\*\*, P < 0.001.

**Fig. 6.** Suppression of DEN/HFD-induced hepatocarcinogenesis by combination of targeting ACLY and PD-L1. (A) Typical appearance of DEN/HFD-induced HCCs subjected to the indicated treatments. (B) Representative tumor sections stained with H&E or immunostained with Ki-67 antibody or oil red O staining. Scale bars, 50  $\mu$ m. (C-I) tumor nodule number (C), tumor volumes (D), Liver weights (E), fatty acids levels (F), TG levels (G), ATP levels (H) and ROS levels (I) from Figure 6A. (J) Expression of TNF $\alpha$ , IL-1 $\beta$ , and IL-6 transcripts in tumors with ETC1002 and ETC1002 synergy with anti-PD-L1 therapy. (K and L) The TNF $\alpha$  and IL-6 levels of Serum (K) and liver (L) in mice with ETC1002 and ETC1002 synergy with anti-PD-L1 therapy. Data were presented as mean  $\pm$  SD. \*P < 0.05, \*\*P < 0.01, \*\*\*P < 0.001.

**Fig. 7.** The IKK $\beta$ -USP30-ACLY axis is upregulated in human HCCs. (A and B) Relative protein levels of IKK $\beta$ , USP30, P-ACLY and ACLY in HCC and their adjacent normal liver tissues from HCC patient samples. (C) Fatty acids levels in HCC and their adjacent normal liver tissues from HCC patient samples. A-C: The horizontal lines in the box plots represent the median, the boxes represent the interquartile range, and the whiskers represent the minimal and maximal values. Significance was performed using Wilcoxon signed rank test. (D and E) Correlation of different protein levels in HCC tissues. (F) Correlation of IKK $\beta$  protein levels with fatty acids levels. (G) Correlation of USP30 protein levels with fatty acids levels. D-G: Each point is an individual sample. R, Spearman correlation coefficient. (H) Schematic diagram of the IKK $\beta$ -USP30-ACLY axis in HCC. IKK $\beta$  phosphorylates USP30 and ACLY. This stabilizes the former protein and promotes the deubiquitination of the latter. USP30 promotes lipid synthesis and inflammation thereby leading to and supporting hepatocarcinogenesis. The combined pharmacologic inhibition of ACLY and PD-L1 inhibits tumor formation.

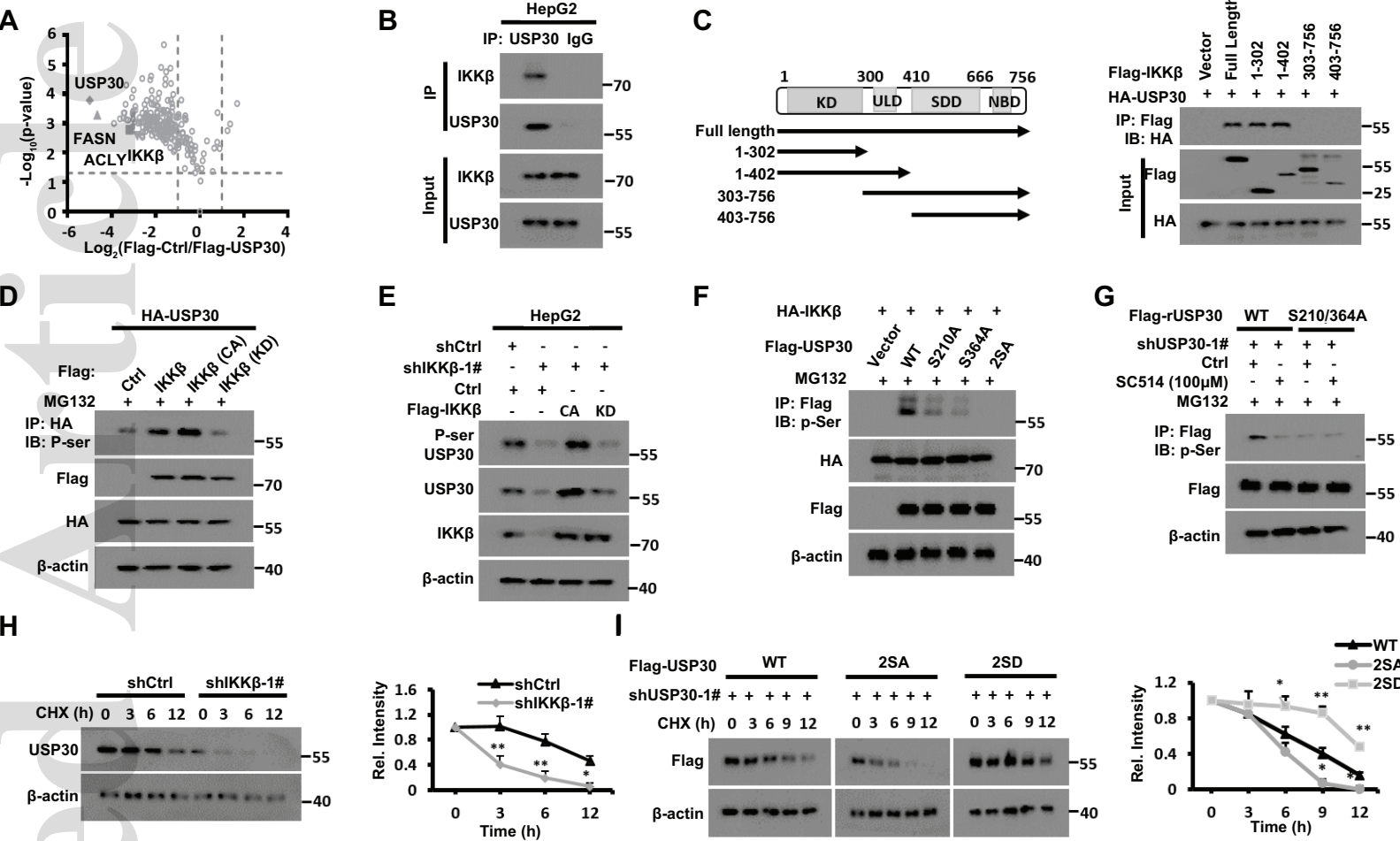
Figure 1



hep\_31249\_f1.eps

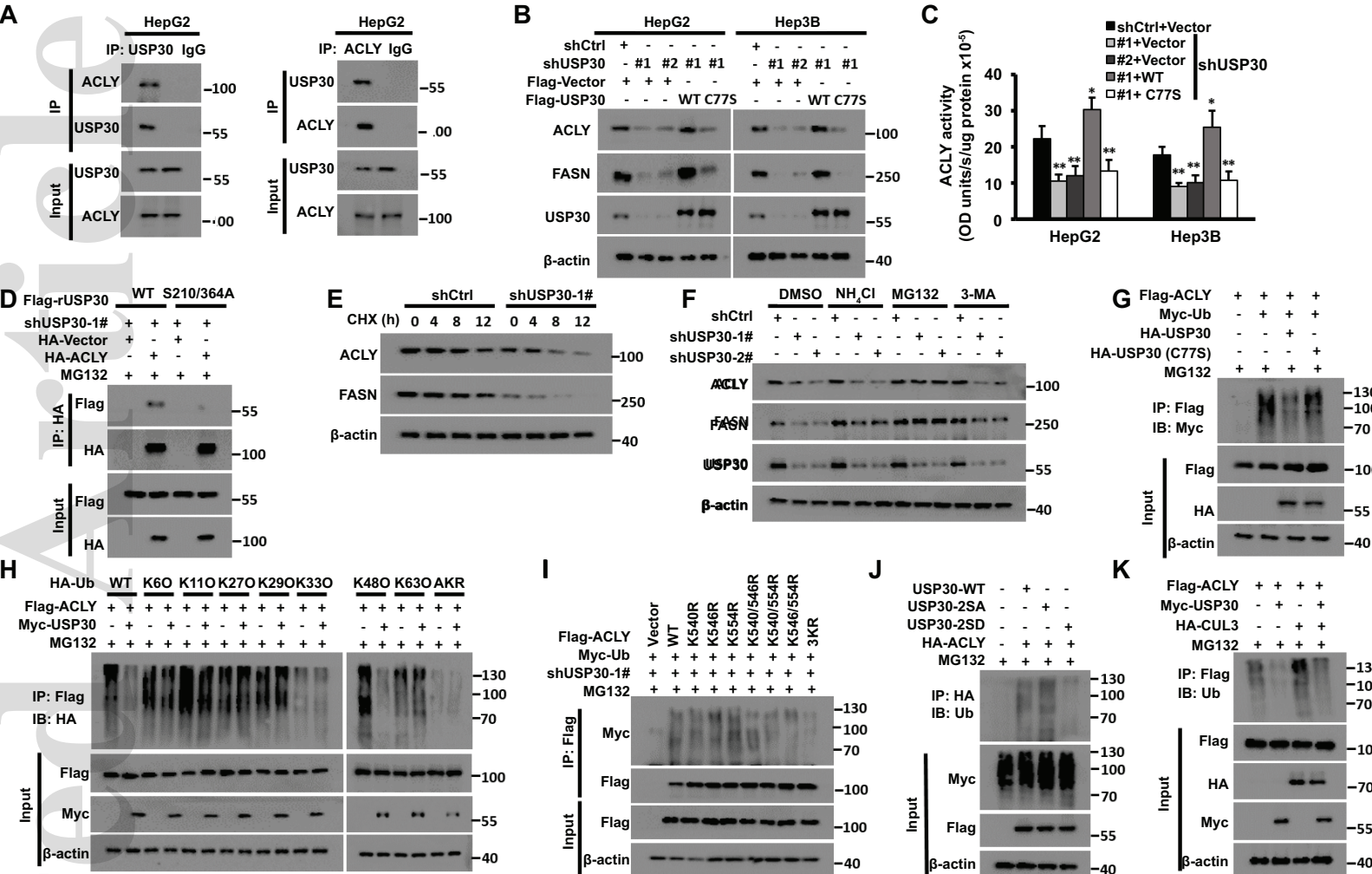
Accepted Article

Figure 2



hep\_31249\_f2.eps

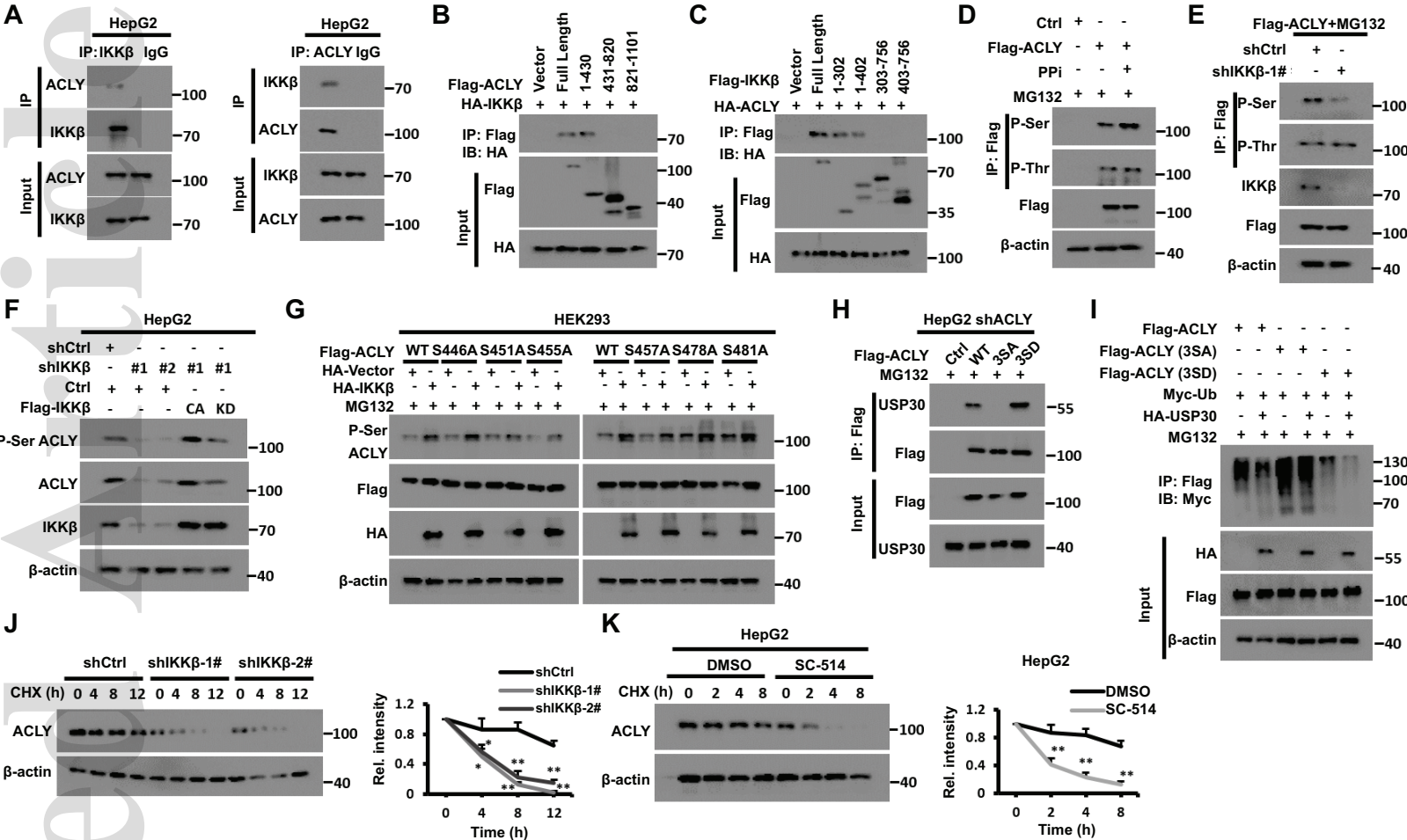
Figure 3



hep\_31249\_f3.eps

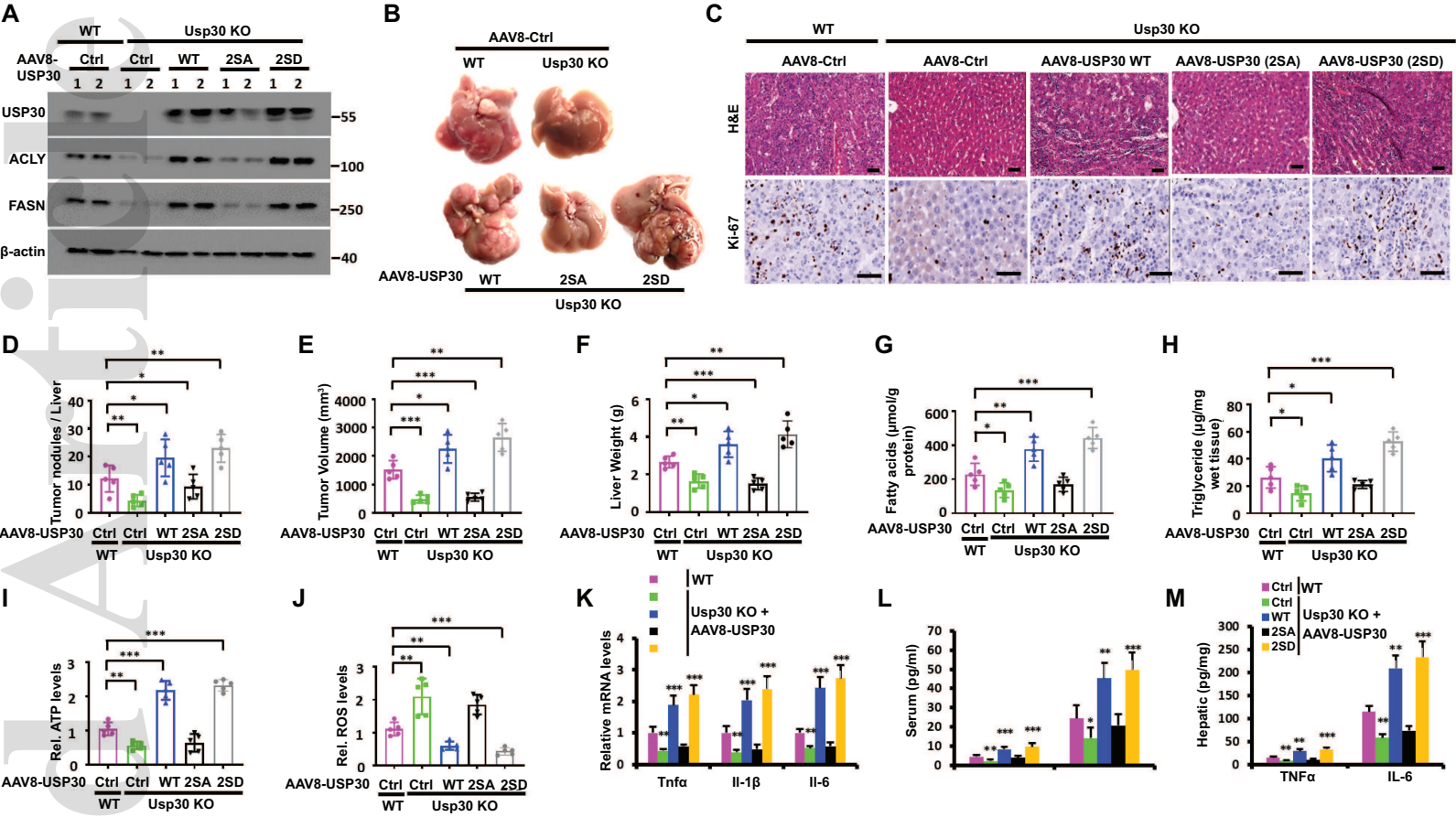
Accept

Figure 4



hep\_31249\_f4.eps

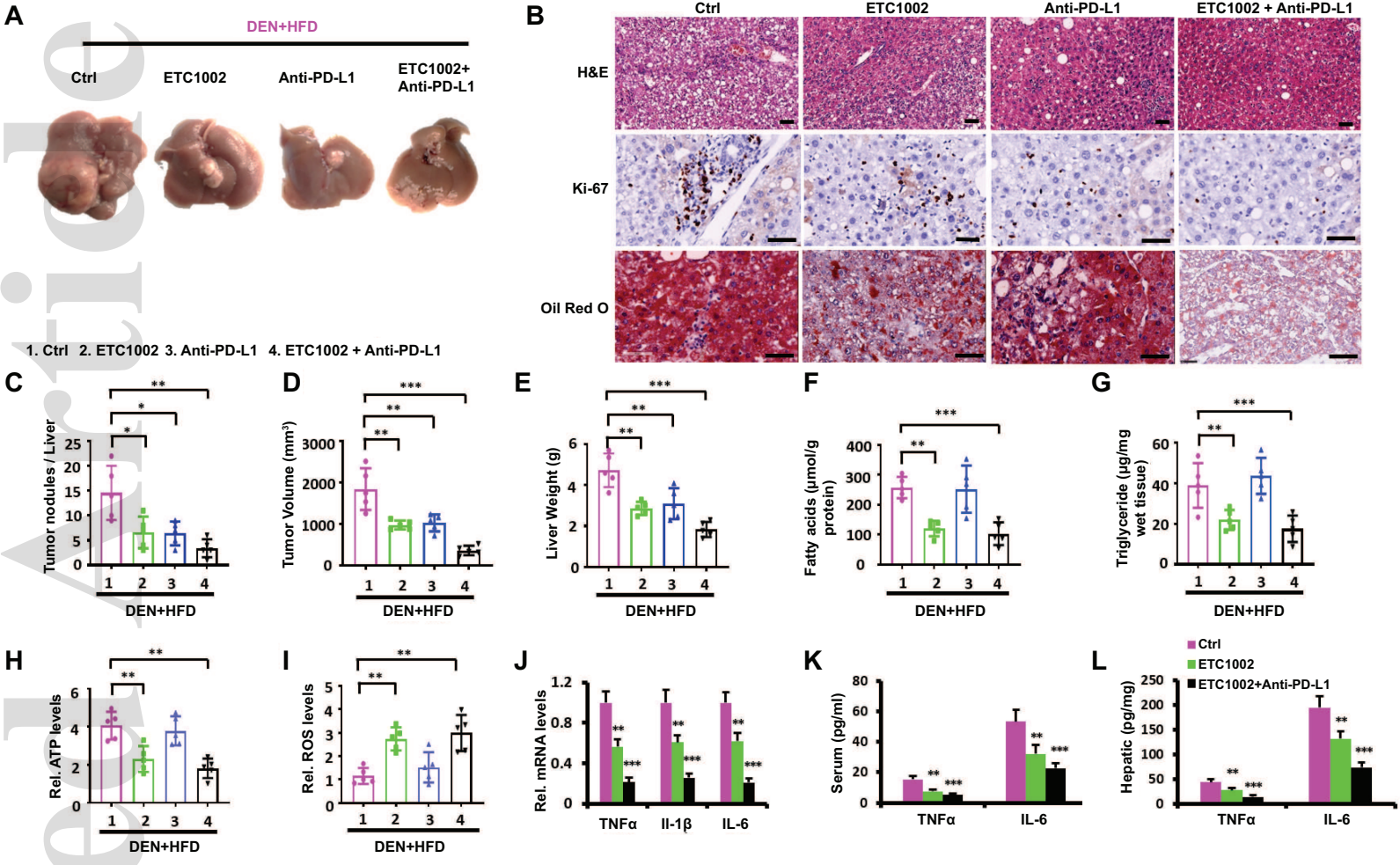
Figure 5



hep\_31249\_f5.eps

Accepted Article

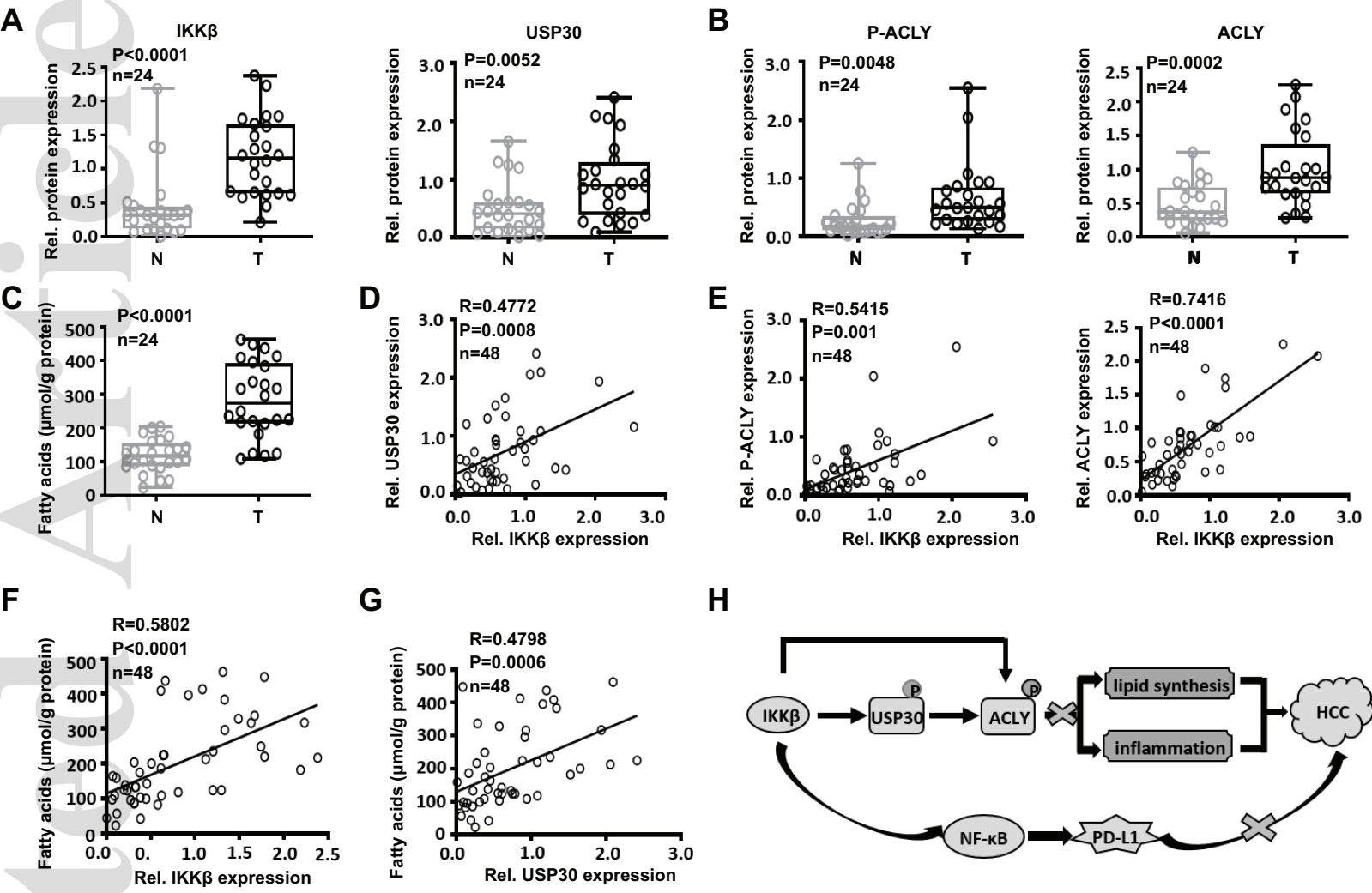
Figure 6



hep\_31249\_f6.eps

Accepted Article

Figure 7



hep\_31249\_f7.eps

Accepted Article